Bottom-inlet-type micro-electro-mechanical system acoustic sensors based on two polyimide/amorphous-Si sacrificial layers

Jaewoo Lee[1,2], Changhan Je[1], Yi-Gyeong Kim[1], Sung Q Lee[1], Woo-Seok Yang[1], Sang-Gug Lee[2]

[1]*Nano Sensor Lab, Electronics and Telecommunications Research Institute, Daejeon 305-700, Republic of Korea*
[2]*Department of Electrical Engineering, Korea Advanced Institute of Science and Technology, Daejeon 305-701, Republic of Korea*
E-mail: jaewoo@etri.re.kr

Published in Micro & Nano Letters; Received on 30th June 2014; Revised on 5th September 2014; Accepted on 23rd September 2014

A bottom-inlet-type micro-electro-mechanical system acoustic sensor based on two polyimide/a-Si sacrificial layers is presented. A diaphragm was adapted to be on the top side of the sacrificial layers, showing the bottom-inlet structure for the package, which has the sensitivity of more than 3 dB compared with that of the top-inlet type. Also, the fundamental CMOS process implemented with Al electrodes was applied to have simple releasing steps by O_2 ashing and XeF_2 isotropic etching because of their material etching selectivity. The sensor module had a sensitivity of −38.9 dBV/Pa at 1 kHz with a bias of 9.2 V in the sweep range from 100 Hz to 16 kHz. In addition, to evaluate the open-circuit sensitivity, structure-based equivalent circuit modelling was performed with lumped parameters. The modelled sensitivity was in good agreement with the measured sensitivity in the error rate of 4.3% under 8 kHz, demonstrating the validity of the modelling. The modelled open-circuit sensitivity was determined to be −37.2 dBV/Pa at 1 kHz using the proposed lumped model.

1. Introduction: The market-share of micro-electro-mechanical system (MEMS) microphones has been steeply increasing against electret condenser microphones (ECMs), especially for mobile application, owing to their matured technology. Smartphones usually require more than two microphones, but the area for multiple microphones is tightly limited to some extent. For miniaturisation, MEMS microphones capable of being scaled down are highly competitive. As a result, they have been applied [1–8] in the real field on the basis of surface and bulk micromachining, as MEMS microphones fabricated through a semiconductor process can be directly applied to surface-mounted technology for packaging on account of their high thermal stability as well as miniaturisation. Most MEMS microphones are designed to have a diaphragm on the bottom side over a substrate, featuring a flat diaphragm structure and an easy application of the deep-reactive ion etching (DRIE) process on the back side of the substrate because of high etching selectivity. Subsequently, this conventional formation makes the package the top-inlet type, which means that the input acoustic pressure can be applied through the port of the metal lid rather than the bottom port of the printed circuit board. Moreover, for protection of the diaphragm against dust or other materials except the acoustic pressure, the back-plate must be on the front end opposite the inlet. However, the sensitivity of the conventional top-inlet scheme is 3 dB lower than that of the bottom-inlet type because of the indirect acoustic pressure forcing. Thus, to improve the sensitivity of the conventional package structure, the diaphragm should be on the top side, having the bottom-inlet type for the package. In addition, an oxide layer is usually implemented as a sacrificial layer in MEMS microphones because of the high etching selectivity for HF etchant between oxide and silicon. Consequently, the oxide layer is strongly tied with the usage of poly-silicon for the two electrodes, having some limitations for selection of electrode materials such as Al or TiN. Despite this common application, it can lead to complications in the fabrication process. To overcome these problems, one solution may be to find sacrificial layers suitable for the fundamental CMOS process to simplify the fabrication process with consideration of etching selectivity using O_2 ashing and XeF_2 isotropic etching methods.

In this Letter, to meet the requirements of mass production and to improve cost and technology competitiveness, a new bottom-inlet-type MEMS acoustic sensor based on two polyimide/amorphous-Si (a-Si) sacrificial layers is proposed. Moreover, for accurate evaluation, structure-based equivalent circuit modelling based on the parameter extraction method is implemented to obtain the frequency characteristics [2, 3, 9].

2. Design

2.1. Diaphragm design: The proposed bottom-inlet-type MEMS acoustic sensor is shown in Fig. 1. It consists of a movable $Al/Si_3N_4/Al$ diaphragm, a fixed back-plate and a back-plate anchor. The movable diaphragm is supported by either multiple diaphragm arms or a single circular arm on the side, and it is placed over the rigid back-plate with an air gap. Each arm for the diaphragm has to be formed in such a way as to lower the spring

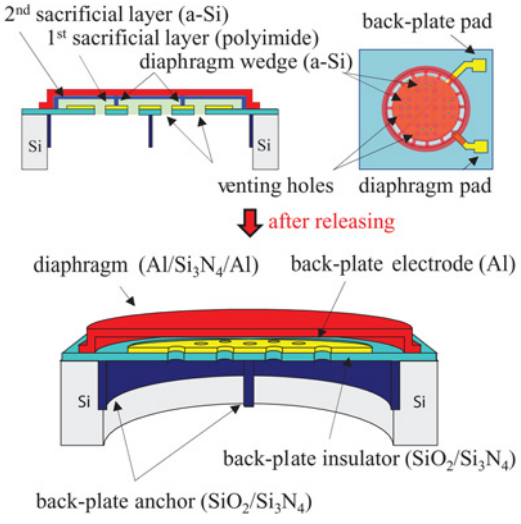

Figure 1 *Schematic views of the MEMS acoustic sensor with two sacrificial layers*

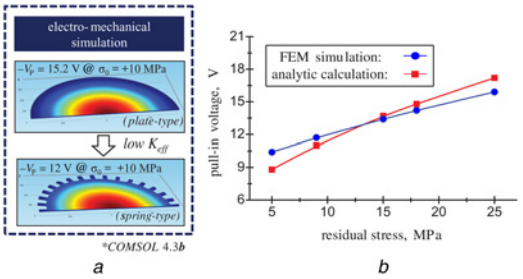

Figure 2 *Pull-in voltage design for the proposed MEMS acoustic sensor*
a FEM simulation results
b Comparison of the results with analytic data for the pull-in voltage

constant of the diaphragm, thus enhancing the open-circuit sensitivity. Also, to improve the frequency response, the back-plate anchor with wheel-shaped inner cross bars was placed and fixed underneath the back-plate using DRIE patterning. Each cross bar's pattern width was 1.5 μm, which was surrounded by an outer circle of 670 μm diameter. The outer circle's 30 μm-deep wall, which was the definition pattern of the back chamber, prevented the foundation of the diaphragm anchors being etched by XeF_2. The back-plate anchor pattern was filled by the back-plate layer composed of oxide and nitride layers of 2.3 μm. In the back-plate, the diameter of each back-plate hole was 8.0 μm. Fig. 2*a* shows the schematics of the pull-in voltage (V_P) of the Al/Si_3N_4/Al diaphragm modelled by finite element method (FEM) simulation using COMSOL Multiphysics 4.3b. The spring-type diaphragm was adapted to have a lower pull-in voltage, whose value of V_P was 12 V at the residual stress of +10 MPa. The V_P difference of 3.2 V between the spring and the plate types on the condition of the same residual stress must be considered for the design issues; therefore the MEMS sensor had a diaphragm of 650 μm diameter and 32 diaphragm anchor arms, where each arm had the width of 20 μm and the length of 40 μm. Moreover, for the spring type, the pull-in voltages were investigated in comparison with the simulation results by an analytic calculation. The pull-in voltage can be expressed as follows [10]

$$V_P = \sqrt{\frac{\left(\left(64D/a^4\right)+\left(4\sigma h/a^2\right)\right)\left(d_0/3\right)+\left(128\alpha D/h^2a^4\right)\left(d_0/3\right)^3}{\varepsilon_0\left(\left(5/6d_0^2\right)+\left(4/3\pi a d_0\right)+\left(1.918/\pi a^2\right)\right)}} \quad (1)$$

where h is the membrane thickness, D is the flexural rigidity, d_0 is the air-gap height, σ is the residual stress, ε_0 is the air dielectric constant and α is the Poisson ratio-dependent empirical parameter. The FEM simulation results in the range of +5 to +30 MPa residual stress are in agreement with the calculation by (1), as shown in Fig. 2*b*. The dependency of the pull-in voltage on the residual stress is similar for both cases from 9.0 to 18.0 V under the same stress condition. Thus, with the modelled data, the effective residual stress from the measured V_P can be tailored or extracted for a specific design.

2.2. Sacrificial layer design: Except oxide, other materials, such as a-Si or polyimide, can be used as a sacrificial layer allowing two electrodes for capacitive sensors to be formed from Al, Ti or TiN; the fabrication process is simple because of simultaneous patterning of the back-plate electrode with the probe pads. Also, if HF is not used to remove the sacrificial layer, material selectivity is greatly increased and the fundamental CMOS processes based on O_2 ashing and XeF_2 etching can be easily applied. Hence, two sacrificial layers were selected: a-Si and polyimide, which indicates that the two electrodes would be

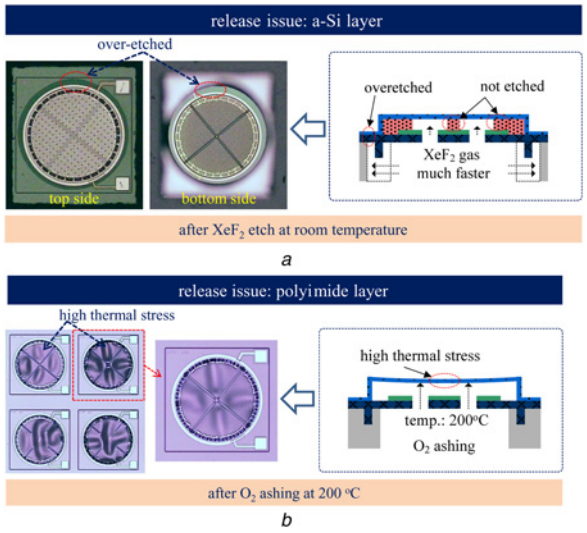

Figure 3 *Images for fabrication issues of using a single sacrificial layer scheme: a-Si and polyimide*
a a-Si
b Polyimide

implemented by Al. Initially, to fabricate the Al electrodes including two connection pads related with the read-out IC (ROIC), only one sacrificial layer was only used. For the a-Si case, the deposition conditions of PECVD a-Si (thickness: 2 μm, mean compressive stress: −40 MPa, only SiH_4: 300 sccm, pressure: 1.0 torr, power: 120 W in P-5000 Mark II) was adopted. When the XeF_2 etching process was applied, the XeF_2 gas was not able to penetrate through the sacrificial layer because of the different etching rate, resulting in deep side wall etching of the back chamber rather than the narrow sacrificial layer as shown in Fig. 3*a*. Clearly, there must be a pass for XeF_2 gas for completing the releasing. Owing to easy releasing by O_2 ashing, a polyimide was applied to the sacrificial layer. The polyimide produced by DuPont (model: PI2545) had a tensile residual stress of +20 MPa after curing at 400°C with a film thickness of 2 μm. Despite thorough removal of the polyimide sacrificial layer, the topology of the diaphragm suffered from severe deformation as shown in Fig. 3*b*. Both the high coefficient of thermal expansion (CTE) of Al (~23) and low residual stress may cause the topology to deviate from the initial gap height. Therefore, a-Si on the polyimide layer was stacked to ensure that there would be no deformation of the diaphragm after the releasing process, where the diaphragm wedges were located in the first patterned sacrificial layer as shown in Fig. 4. The wedges with a diameter of 1 μm were formed with regular spacing of 78 μm at the same time as the second sacrificial layer was deposited. While the first sacrificial layer was removed by O_2 ashing at 200°C, the diaphragm wedges worked as rigid pins that prevented the

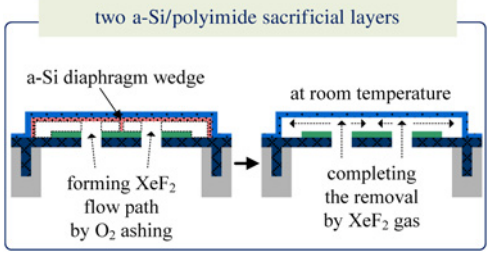

Figure 4 *Schematic concepts of two sacrificial layers for the proposed MEMS acoustic sensor*

doi: 10.1049/mnl.2014.0381

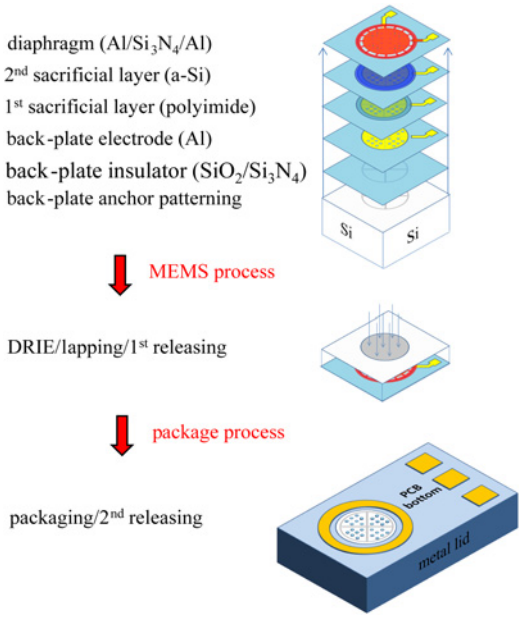

Figure 5 *Schematic views of each fabrication process including the packaging process for the MEMS acoustic sensor*

diaphragm from deflecting against the high thermal load. Therefore, because of the excellent etching selectivity of the XeF_2 etchant on Si against organic materials, the final releasing step of a-Si can be carried out after the packaging process.

3. Fabrication: The fabrication process for the implementation is shown in Fig. 5. The MEMS process and the standard ETRI 0.8 µm CMOS process on a Si substrate of 675 µm thickness were applied in the fabrication of the MEMS acoustic sensor. First, using DRIE, a back-plate anchor was patterned on a-Si substrate, which could work as a passivation layer against the XeF_2 etchant. After patterning, it was filled with a multi-layer back-plate, in which the layers comprised 1.0 µm of thermal SiO_2 (Diffusion Furnace E1550 HT, 1000°C, mean compressive stress: −310 MPa) and 0.8 µm of LPCVD Si_3N_4 (Diffusion Furnace E1550 HT, 800°C, mean compressive stress: −10 MPa). The back-plate electrode was a 0.5 µm-thick layer of Al (Varian Sputter *M2i*, mean tensile stress: +150 ~ +250 MPa). After that, a 1.2 µm layer of polyimide was deposited as the first sacrificial layer, and a 1.0 µm layer of a-Si was deposited and patterned as the second sacrificial layer. A diaphragm of $Al/Si_3N_4/Al$ layers was fabricated with a total thickness of 0.6 µm. The multi-layer structure was used to compensate for the residual stress of each layer. The Al layer deposited by sputtering generally has tensile stress, whereas the Si_3N_4 layer in PECVD can be easily handled with a portion of NH_3 gas over a wide range of stresses from tensile stress to compressive stress. Thus, we chose the multi-layer scheme to form a near stress-free diaphragm. Moreover, in the standard CMOS processes, Al is very commonly used as an electrode. Therefore, using polyimide as a sacrificial layer, we were able to use Al as an electrode of the diaphragm without any limitation of the fabrication process margin. After the back chamber was etched to 675 µm by DRIE and the substrate was lapped to 400 µm thickness because of the limitation of package height, the first sacrificial layer was removed by O_2 ashing at 200°C.

After packaging, the fabrication process was finally completed with the removal of the second sacrificial layer by an isotropic XeF2 etchant. Fig. 6 shows scanning electron microscopy (SEM) images of the top and bottom views of the fabricated MEMS acoustic sensor. The back-plate had four cross patterns as shown in the

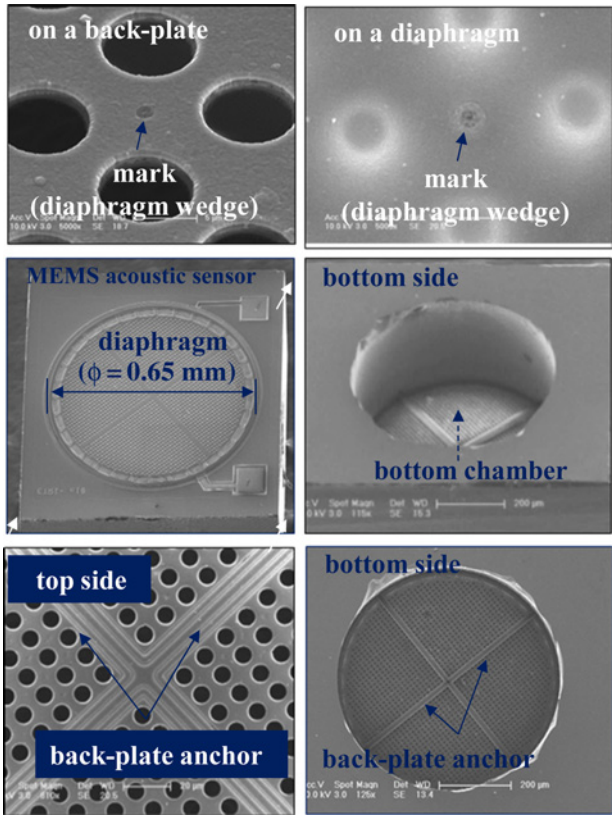

Figure 6 *SEM images of the diaphragm and the back-plate of the fabricated MEMS acoustic sensor*

upper part. In addition, to handle the air resistance between two electrodes, the back-plate was perforated with 1955 acoustic holes, which were also used as etching holes to remove the sacrificial layer. The acoustic sensor had a chip area of 1.0 × 1.0 mm, and its chip thickness was 400 µm.

4. Characterisation: The C–V characteristic for the pull-in voltage is shown in Fig. 7. With the measured pull-in voltage of 10.8 V, the effective residual stress on the basis of the analytic calculation result was determined to be a tensile stress of +8.5 MPa. Fig. 8*a* shows the packaged MEMS microphone module composed of a MEMS acoustic sensor and the ROIC, where the dimensions of the microphone package were 3.4 × 2.5 × 1.0 mm. The characterisation was performed in an anechoic chamber with a commercial analysis set (B&K 3560 and 7700). The measured sensitivity (S_{mea}) and noise level (A-weighted) of the packaged microphone were −38.9 dBV/Pa at 1 kHz (0 dB = 1 V/Pa) and −96.8 dBV, respectively, where the ROIC had 0.6 pF input capacitance (C_{in}), 9.2 V output bias, 6 dB gain (G) and 0.4 pF

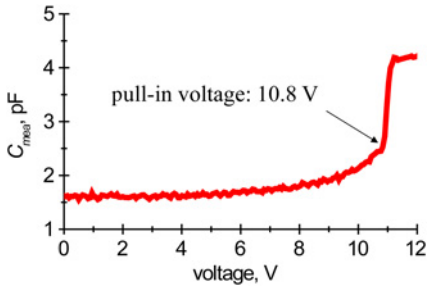

Figure 7 *Measured pull-in voltage characterisation of the proposed MEMS acoustic sensor*

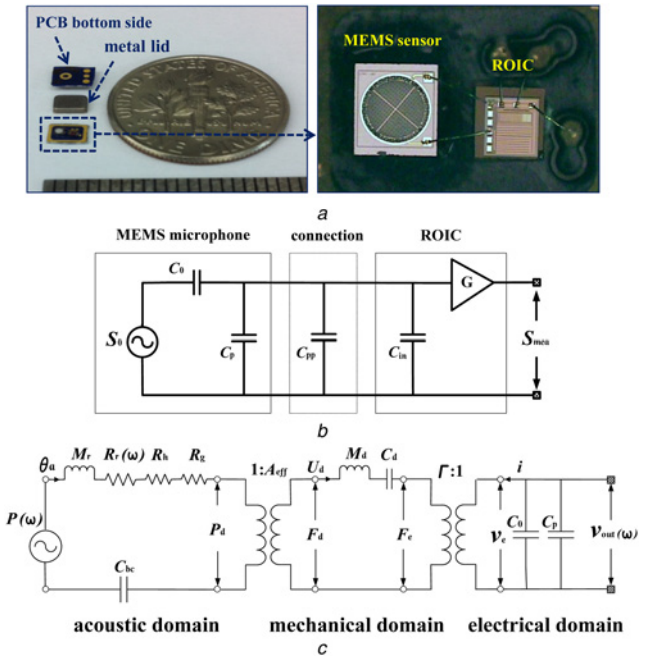

Figure 8 *Fabricated MEMS microphone and analogous equivalent circuits*
a Packaged MEMS microphone module
b Electrical circuit block diagram for measured sensitivity (S_{mea})
c An equivalent circuit model describing the interaction between the parameters in the three signal domains

connection capacitance (C_{PP}). To obtain the open-circuit sensitivity (S_o) as shown in Fig. 8*b*, it was extracted from S_{mea} by (2)

$$S_{mea} = S_0 \cdot \frac{C_0}{C_0 + C_P + C_{PP} + C_{in}} \cdot G \tag{2}$$

where the zero-bias intrinsic capacitance (C_0) was 1.2 pF, and the parasitic capacitance (C_P) was 0.75 pF. From (2), the S_o was extracted as −37.1 dBV/Pa. To evaluate the characteristics of the MEMS acoustic sensor, structure-based equivalent circuit modelling was performed with lumped parameters, which included both empirical and theoretical data. In the structure model shown in Fig. 8*c*, a sound pressure (P) as an input signal is generally transduced to an electrical voltage (V_{out}) as an output signal on the output capacitance, resulting in S_o by Tilmans [9]

$$S_0 = \frac{v_{out}(\omega)}{P(\omega)} = \frac{1}{A_{eff} \cdot K_1(\omega) + (1/A_{eff}) \cdot K_2(\omega)} \cdot \frac{\Gamma}{j\omega(C_0 + C_P)} \tag{3}$$

Table 1 Measured and modelled parameters

Model parameters	Values
radius of the diaphragm (r)	3.25×10^{-4} m
effective area of the diaphragm (A_{eff})	1.11×10^{-7} m^2
effective spring constant (K_{eff})	24 N/m
effective mass of the diaphragm (m_{eff})	2.10×10^{-10} kg
intrinsic capacitance (C_O) at V_{bias}[a]	1.20 pF
parasitic capacitance (C_P) at V_{bias}[a]	0.75 pF
air-gap height (d_0)	2.0 µm
air-gap height (d_{eff}) at V_{bias}[a]	1.8 µm
effective residual stress of the diaphragm (σ_0)	+8.5 MPa
damping coefficient (b_c) at V_{bias}[a]	4.62×10^{-5} kg/s
transduction factor of mechanical-electric coupling (Γ)	5.78×10^{-6} c/m

[a]Bias condition (V_{bias}) = 9.2 V

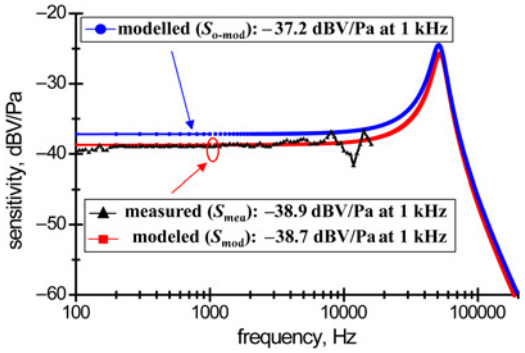

Figure 9 *Modelled and measured sensitivities (S_{mea}, S_{mod}) and modelled open-circuit sensitivity ($S_{o\text{-}mod}$) against frequency for the proposed MEMS acoustic sensor*

where $K_1(\omega)$ and $K_2(\omega)$ are given by

$$K_1(\omega) = R_r(\omega) + R_h + R_g + j\omega M_r + \frac{1}{j\omega C_{bc}} \tag{4}$$

$$K_2(\omega) = j\omega M_d + \frac{1}{j\omega C_d} + \frac{\Gamma^2}{j\omega(C_0 + C_P)} \tag{5}$$

Here, θ_a is the volume velocity, M_r is the mass of the air close to the diaphragm, $R_r(\omega)$ is the radiation resistance of the diaphragm, R_g is the viscous resistance of the air-gap, R_h is the viscous resistance of the acoustic holes, C_{bc} is the compliance of the back chamber, and P_d is the diaphragm portion of the input pressure that is converted to the related force in the mechanical domain, F_d is the force transformed to the mechanical domain, A_{eff} is the transformer ratio in the acoustic and mechanical coupling, U_d is the velocity, θ_d is the volume velocity at the diaphragm that is equal to θ_a, M_d is the mass of the diaphragm, C_d is the compliance of the diaphragm, F_e is the intrinsic capacitance portion of the converted force, v_e is the voltage transformed to the electrical domain, Γ is the transformer ratio in the electromechanical coupling, i is current and v_{out} is the output voltage. Γ denotes the relationship of the total static charge divided by the air-gap height with the intrinsic capacitance. Each parameter for the model is given in Table 1. Compared with the measured sensitivity (S_{mea}), the modelled result (S_{mod}) shown in Fig. 9 verified the validity of the structure-based equivalent circuit modelling. S_{mod} was in good agreement with S_{mea} with the error rate of 4.3% under 8 kHz. It must be noted that because of a noise factor of an evaluation board, the characteristic of S_{mea} fluctuated highly rather than the flat response in the high-frequency range from 8 to 16 kHz, degrading the modelling performance. The modelled open-circuit sensitivity ($S_{o\text{-}mod}$) was determined to be −37.2 dBV/Pa at 1 kHz using the proposed lumped model. Also, regarding the dependency of the frequency response on bias points, the values of $S_{o\text{-}mod}$ at 6.0, 7.0 and 8.0 V were −41.9, −40.2 and −38.8 dBV/Pa, respectively.

5. Conclusion: A bottom-inlet-type MEMS acoustic sensor using two polyimide/a-Si sacrificial layers is newly presented. The structure enables the topology of the diaphragm to be sustained without deformation during the releasing process, and it shows good thermal characteristics. Also, because HF is not used for oxide release, the fabrication process is much simpler than the conventional process. In addition, to achieve open-circuit sensitivity, equivalent circuit modelling was performed, and the validity of the proposed design was demonstrated.

6. Acknowledgments: This work was supported by the IT R&D programme of MKE/KEIT (10035570, Development of

doi: 10.1049/mnl.2014.0381

Self-Powered Smart Sensor Node Platform for Smart and Green Building).

7 References

[1] Scheeper P.R., var der Donk A.G.H., Olthuis W., Bergveld P.: 'A review of silicon microphones', *Sens. Actuators A*, 1994, **44**, pp. 1–11

[2] Wang W.J., Lin R.M., Zou Q.B., Li X.X.: 'Modeling and characterization of a silicon condenser microphone', *J. Micromech. Microeng.*, 2004, **14**, pp. 403–409

[3] Gato M., Iguchi Y., Ono K., *ET AL.*: 'High-performance condenser microphone with single-crystalline silicon diaphragm and backplate', *IEEE Sens. J.*, 2007, **7**, pp. 4–10

[4] Lee J., Je C.H., Jeon J.H., Yang W.S., Kim J.: 'A surface micromachined MEMS acoustic sensor with back-plate anchors of 100 μm depth'. IEEE Sensor Conf., October 2011, pp. 1978–1981

[5] Fraux R.: 'Knowles SPM0408HE5H MEMS microphone'. Reverse Costing analysis, SYSTEMPlus Consulting, ver 1, September 2009

[6] Hallereau S.: 'AAC Acoutic iPhone 4 MEMS microphone'. Reverse Costing analysis, SYSTEMPlus Consulting, ver. 1, September 2011

[7] Youle Developpment and SYSTEMPlus Consulting: 'Reverse engineering and costing of a family of MEMS microphones – Analysis of each device, technology and production cost comparison', 2012

[8] Lee J., Je C.H., Yang W.S., Kwon J.K.: 'Bottom-inlet-type MEMS acoustic sensors based on two polyimide/a-Si sacrificial layers'. APCOT 2014, June 2014

[9] Tilmans H.A.C.: 'Equivalent circuit representation of electromechanical transducers: I. Lumped-parameter systems', *J. Micromech. Microeng.*, 1996, **9**, pp. 157–176

[10] Rahman M., Chowdhury S.: 'A highly accurate method to calculate capacitance of MEMS sensors with circular membranes'. IEEE Int. Conf. Electro/Information Technology, 2009, Vol. 9, pp. 178–181